



Review

Systematic Review on Human Skin-Compatible Wearable Photoplethysmography Sensors

Inho Lee ^{1,†}, Nakkyun Park ^{2,†} , Hanbee Lee ¹, Chuljin Hwang ² , Joo Hee Kim ^{2,*} and Sungjun Park ^{1,*} 

¹ Department of Electrical and Computer Engineering, Ajou University, Suwon 16499, Korea; dlsghdjrrk@ajou.ac.kr (I.L.); gksqlfjqql@ajou.ac.kr (H.L.)

² College of Pharmacy, Ajou University, Suwon 16499, Korea; prk104@ajou.ac.kr (N.P.); aki@ajou.ac.kr (C.H.)

* Correspondence: elisekim@ajou.ac.kr (J.H.K.); sj0223park@ajou.ac.kr (S.P.)

† I. Lee and N. Park contributed equally to this work.

Abstract: The rapid advances in human-friendly and wearable photoplethysmography (PPG) sensors have facilitated the continuous and real-time monitoring of physiological conditions, enabling self-health care without being restricted by location. In this paper, we focus on state-of-the-art skin-compatible PPG sensors and strategies to obtain accurate and stable sensing of biological signals adhered to human skin along with light-absorbing semiconducting materials that are classified as silicone, inorganic, and organic absorbers. The challenges of skin-compatible PPG-based monitoring technologies and their further improvements are also discussed. We expect that such technological developments will accelerate accurate diagnostic evaluation with the aid of the biomedical electronic devices.

Keywords: skin electronic; optoelectronic device; photodiodes; phototransistors; PPG sensors; oximeters; health-care platform



Citation: Lee, I.; Park, N.; Lee, H.; Hwang, C.; Kim, J.H.; Park, S. Systematic Review on Human Skin-Compatible Wearable Photoplethysmography Sensors. *Appl. Sci.* **2021**, *11*, 2313. <https://doi.org/10.3390/app11052313>

Academic Editor: Akram Alomainy

Received: 17 February 2021

Accepted: 28 February 2021

Published: 5 March 2021

Publisher's Note: MDPI stays neutral with regard to jurisdictional claims in published maps and institutional affiliations.



Copyright: © 2021 by the authors. Licensee MDPI, Basel, Switzerland. This article is an open access article distributed under the terms and conditions of the Creative Commons Attribution (CC BY) license (<https://creativecommons.org/licenses/by/4.0/>).

1. Introduction

With an aging population, the demand for wearable electronic devices to monitor physiological conditions has increased exponentially in recent years [1–4]. The continuous and real-time measurement of physiological parameters using different sensing techniques plays an important role in diagnosing health conditions. For example, small wearable sensor systems have been developed for people who are at risk of heart attack, seizures, and stroke [5–7]. Wearable devices are also becoming widely used to gather information about an individual's muscle activity, sleep quality, and other physiological activities in daily life [8,9].

Several options for wearable technology have emerged in the form of integrated clothing, accessories, and body attachments [10–14]. A classic example is a photoplethysmography (PPG) sensor which utilizes infrared light to noninvasively measure changes in pulsatile blood flows at the skin surface [15]. At present, the PPG can be applied to various aspects of cardiovascular monitoring, including the detection of arterial oxygen saturation (SpO₂), heart rate, blood pressure, cardiac output, respiration, arterial aging, endothelial function, microvascular blood flow, and autonomic function [16–24].

By applying sensors and mobile computing devices directly onto the body surface, the PPG sensor could also be designed as a skin-on interface [25,26]. The skin-interfaced wearable devices have the advantage of allowing the continuous monitoring of various physiological data as comfortably as possible. Moreover, flexible and stretchable electronic devices can conformally be placed on the skin and detect various signals with extremely high sensitivity [27–29].

Despite the recent advances in wearable sensor technology for clinical applications, the following challenges still remain: (i) skin irritation due to friction between the skin and device; (ii) insufficient conformal adhesion with a complex skin surface owing to the rigidity

of devices; (iii) low operational durability under repetitive mechanical deformation; and (iv) high power consumption for long-term and portable applications, as most photoresponsive semiconducting materials comprise rigid inorganic materials in hard and bulky device architecture. Therefore, crucial considerations are the selection of sensing materials and the skin-integration strategies for PPG sensors to achieve their mechanical and functional properties.

In this paper, we provide a systematic review of the latest developments of PPG technology for clinical applications. A brief overview of the operational mechanism and its applications of PPG sensors is first presented, followed by recent progress and technological developments of skin-compatible materials to obtain accurate and stable light-sensing performance and mechanical durability. Finally, we highlight current challenges and possible future research directions for multifunctional PPG sensors.

2. Methodology

The search strategy was developed according to the guidelines of Preferred Reporting Items for Systematic Reviews and Meta-Analyses. The systematic literature search was performed using the following five databases: PubMed, IEEE Xplore, Web of Science, Google Scholar, and Scopus. All databases were searched for the following terms:

Group A terms: (PPG) OR (Photoplethysmography) OR (Photoplethysmogram) OR (plethysmogram) OR (optometric) OR (optoelectronic).

Group B terms: (blood) OR (heart rate) OR (heart pressure) OR (oximeter) OR (hemoglobin).

Group C terms: (flexible) OR (wearable) OR (portable) OR (stretchable) OR (attachable) OR (electronic skin).

Group D terms: (organic) OR (inorganic) OR (hybrid).

Group E terms: (reflection) OR (transmission) OR (non-invasive).

Groups A, B, C, D, and E were combined. Recent studies published in English in the last five years are considered in this review. Two of the authors (N.P. and I.L.) independently searched the full text, excluding papers that did not meet the selection criteria and did not have full-text access.

The search results are presented in Figure 1 and Table 1. A total of 639 papers were found in five databases. Duplicates and unrelated titles were excluded using EndNote, and 624 papers did not meet the inclusion criteria. After excluding irrelevant papers, 15 papers were selected for this study. The considered PPG devices were divided into four main groups according to fabrication materials: silicone, organic, inorganic, and hybrid.

Table 1. State-of-art skin-compatible and wearable photoplethysmography (PPG) sensors.

| Author | Year | Active Material | Bending Radius (mm) | Oximetry Mode | Photo-Responsive Range (nm) | Ref |
|---------------|------|-----------------------------|---------------------|----------------------------|-----------------------------|------|
| Kim et al. | 2016 | Silicon PIN | - | Reflection | 350–1120 | [30] |
| Kim et al. | 2017 | Silicon PIN | 5 | Reflection | 350–1120 | [31] |
| Li et al. | 2017 | Silicon | - | Reflection | 450–1000 | [32] |
| Kim et al. | 2017 | GaAs | 2.4 | Reflection | 300–900 | [33] |
| Kim et al. | 2017 | PbS QD | 0.035 | Transmission | 400–1100 | [34] |
| Polat et al. | 2019 | Graphene/PbS QD | 16 | Reflection | 300–2000 | [35] |
| Yokota et al. | 2016 | P3HT:PCBM | 0.1> | Reflection | 350–800 | [36] |
| Park et al. | 2018 | PIPCCP:PC ₆₁ BM | 0.003> | Transmission | 300–900 | [37] |
| Khan et al. | 2018 | TMB:BB/PC ₇₁ BM | >100 | Reflection | 400–950 | [38] |
| Khan et al. | 2019 | - | >50 | Reflection | 400–930 | [39] |
| Xu et al. | 2017 | DPP-DTT:PCBM | 9> | Reflection | - | [40] |
| Lee et al. | 2018 | C ₇₀ :TAPC | 4.5 | Reflection | 350–750 | [41] |
| Kim et al. | 2020 | PTB7-Th:PC ₇₁ BM | 3.5 | Transmission Reflection | 400–800 | [42] |

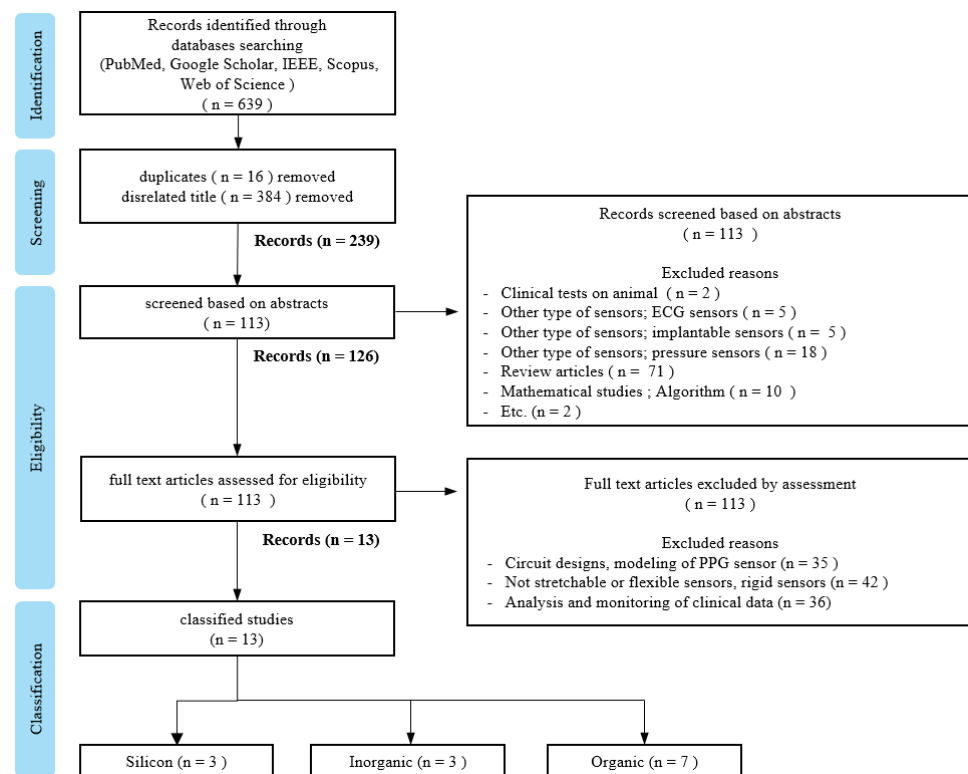


Figure 1. PRISMA flowchart of the identification and selection of studies.

3. Photoplethysmography (PPG) Sensor and Its Application

3.1. Mechanism of PPG Sensor

A PPG sensor is an optically obtained plethysmogram to monitor blood volume changes in the microvascular system. Conventional PPG sensors comprise two main components: light-emitting diodes (LEDs) and photodetectors (PDs). In the device architecture, red and near-infrared light from LEDs has generally been used as the long wavelengths are suitable for measuring deep-tissue blood flow [43]. The PDs detect volumetric changes in blood from cardiac pressure by absorbing light illumination from LEDs through the skin. The noninvasive and optical measurement system enables a PPG to monitor breathing, hypovolemia, and other circulatory conditions [44].

The PPG signal can be acquired in reflection or transmission mode [45]. In transmission mode, the light transmitted through the medium (tissue, bone, and/or blood vessels) is detected, while backscattered or reflected light is detected in the reflection mode. In the PPG sensors' transmission mode, the sensing locations are limited owing to confined transillumination [46]. Therefore, the location of PDs in transmission mode is limited by the thinness of the subject, such as on the fingers, earlobes, and neonatal feet. Conversely, in the reflection mode, the LEDs and PDs are integrated into the same plane, possibly located on various spots, such as the forehead, forearm, abdomen, and legs (Figure 2a).

The PDs can detect changes in light intensity from transmitted and/or reflected light in response to volumetric changes in veins and capillaries. As shown in Figure 2b, the typical PPG waveform consists of direct current (DC) and alternating current (AC) components. The DC component is caused by the absorption of nonpulsating arterial blood and scattering in all tissues, while the AC component is attributed to the volumetric change of arterial blood between systolic and diastolic phases in cardiac cycles [47,48]. The height of the AC signal fluctuates over time due to arterial blood pulsed by the heartbeat.

Pulse oximetry is a revolutionary method for evaluating oxygen saturation levels (SpO_2) using PPG devices. In a theoretical estimation, the oxygen saturation of the arterial blood can be expressed as the amount of oxygenated hemoglobin against the full quantity of hemoglobin:

$$\% \text{SpO}_2 = \frac{\text{HbO}_2}{\text{HbO}_2 + \text{Hb}} \times 100 \% \quad (1)$$

where HbO_2 and Hb are the concentrations of oxy and deoxygenated hemoglobin, respectively. Typically, a pulse oximeter utilizes two different wavelengths of light. One is red and the other is infrared with wavelengths of 660 and 940 nm, respectively. The absorption intensity of light differs significantly depending on the oxygenated condition of hemoglobin. The iron-containing hemoglobin in the red blood cells can bind and transport oxygen during internal respiration. As shown in Figure 2c, the absorption spectra of hemoglobin varied under oxy/deoxygenated conditions. Significantly lower absorption in red (660 nm) light and slightly higher absorption in infrared (940 nm) are observed for oxyhemoglobin compared to deoxyhemoglobin [49]. The red/infrared modulation ratio (R), double-ratio of pulsatile (AC), and nonpulsatile (DC) components in red and infrared light can be used to calibrate the SpO_2 level as follows:

$$R = \frac{\ln \frac{I_{\max,AC}(\lambda_{\text{red}})}{I_{\max,DC}(\lambda_{\text{red}})}}{\ln \frac{I_{\max,AC}(\lambda_{\text{IR}})}{I_{\max,DC}(\lambda_{\text{IR}})}} \quad (2)$$

where A is absorbance. The calculated values of the modulation ratio R correspond to the SpO_2 level. Considering low oxygenated conditions, for example, the amplitude of the AC component in the red-light region decreases compared to its behavior in the IR light region owing to the relatively higher absorption coefficient of deoxyhemoglobin at 660 nm (Figure 2c), resulting in a low R -value.

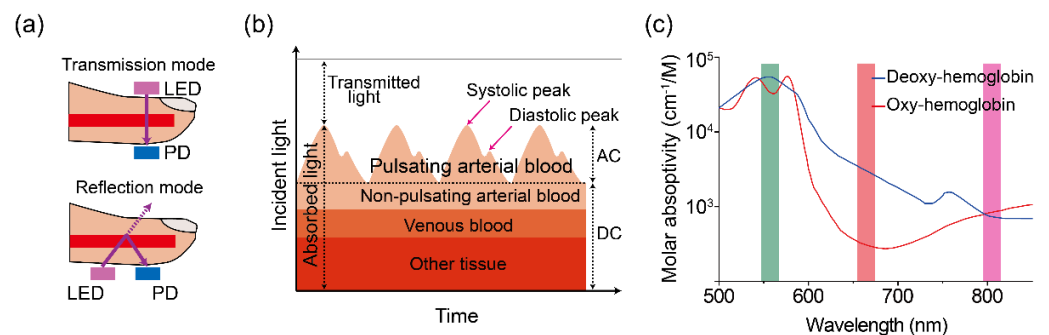


Figure 2. (a) Illustration of a two-mode (transmission and reflection) PPG sensor. (b) Variation in tissue light attenuation. (c) Molar absorptivity of oxygenated (blue line) and deoxygenated (red line) hemoglobin in arterial blood as of wavelength. Reproduced with permission from [50,51], ELSEVIER (1997) and SPIE (1999).

3.2. Applications of PPG Sensor

In clinical practice, the accurate measurement of the clinically relevant hemoglobin derivatives and bilirubin levels can provide useful diagnostic information. Figure 3 shows the absorption spectra of hemoglobin derivatives and bilirubin that can be further studied using skin-compatible PPG sensors.

Methemoglobin (MetHb), along with carboxyhemoglobin (COHb) and sulfhemoglobin (SHb), represents a dyshemoglobin that does not bind O_2 . Normally, only small traces of MetHb and carboxyhemoglobin (COHb) are found in the blood, while sulfhemoglobin (SHb) is absent [52,53]. However, levels of MetHb and COHb are often elevated in severely ill patients, including clinical hypoxia [54], exposure to certain toxic agents [55], smokers [56], and the lack of genetic reductase [57].

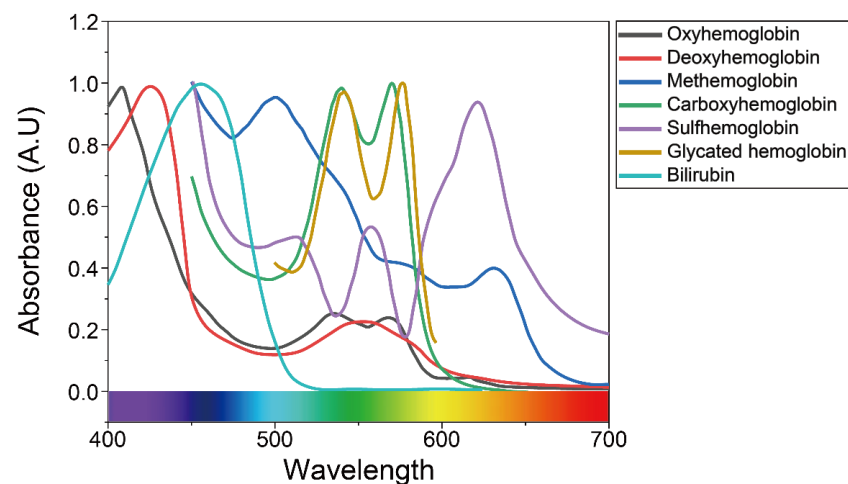


Figure 3. Absorbance of bilirubin and various types of hemoglobin in the visible light region, as mentioned in previous studies. Reproduced with permission from [58–60], ELSEVIER (1981), SPIE (2012), and ACS Publications (2016).

Several observational studies reported the benefits of the continuous monitoring of MetHb and COHb levels to identify patients with carbon monoxide poisoning at triage in the hospital emergency departments [61–63]. Unlike MetHb, which is reversible with an antidote, methylene blue [64], SHb is an irreversible form of oxidized hemoglobin resulting from the incorporation of a sulfur atom in its porphyrin ring [65,66]. Currently, devices such as co-oximeters and blood gas analyzers are used to detect the abnormal presence of MetHb and SHb in blood samples [67,68]. However, the detection tests are not performed routinely in most intensive care units due to cost. The readings provided by those devices are not reliable, giving a false-positive result for methemoglobinemia [69]. Therefore, the noninvasive and low-cost approaches in the detection of MetHb and SHb at the point-of-care would be useful for the early detection of cyanotic conditions. Glycated hemoglobin (HbA1c), which is formed by the binding of hemoglobin, reflects the average blood glucose level over the preceding 60 days [70]. A range of studies [71–74] have demonstrated the benefits of point-of-care HbA1c testing, and the rapid availability of HbA1c testing has been shown to facilitate safe and effective diabetes management. Bilirubin levels are routinely monitored in cases of neonatal jaundice to identify hyperbilirubinemia and to prevent bilirubin-related neurotoxicity [75,76]. Many laboratory devices and methods are available to measure bilirubin levels in the blood. However, results are obtained 24 h after testing leading to delays in treatment. Thus, there is an important need for an accurate point-of-care system that allows rapid and appropriate treatment.

For the continuous and accurate evaluation of health status, securing stable adhesion between the light-responsive active components of PPG sensors and the target surfaces is crucial by minimizing motion artifacts [77]. Additionally, the devices percutaneously monitoring biometric signals require avoidance of toxicity, electric shock, electrolysis, and excessive thermogenesis [78]. To improve these problems, it is necessary to focus on the development of materials. In the next section, an innovative strategy for human skin-compatible PPG sensors depending on different types of light-absorbing semiconducting materials is highlighted.

4. Human Skin-Compatible PPG Sensors

4.1. Silicon Photodiodes

Silicon photodiodes are widely available, cost-effective [79], and nontoxic [80] electronic devices, with light-responsive properties from the UV range (190 nm) to the infrared spectral region (1100 nm) [81]. In addition to their miniature size and high response speeds, they are suitable for both civilian and defense-related applications [82]. In this section, the basic considerations in the design of skin-compatible PPG sensors using Si-PDs are discussed. Additionally, their relative advantages and limitations based on device architectures are highlighted.

Kim et al. reported a battery-free epidermal oximeter with near-field communication (NFC) wireless communication [30], as shown in Figure 4a. An active device is composed of a silicon PIN photodetector with red and infrared LEDs connected for amplifying circuits and a coil for transmitting power and data by magnetic induction. The components are monolithically integrated on elastomeric substrates using serpentine-shaped interconnects with widths of 60–90 μm and a thickness of 5 μm . The integrated devices are located at the neutral plane by encapsulation with physical and electrical isolation. It was confirmed that these devices can maintain operational stability even after stretched condition and can be synchronized with a smartphone at 2 cm, owing to the low flexural rigidity of the metal interconnects. For oximeter applications, the devices are laminated on black textiles coated with a silicone elastomer. The systolic peak and diastolic notch were observed with a sampling rate resolution of 25 Hz. To confirm whether the developed oximeter can be applied in diagnostic applications, an assessment for peripheral vascular diseases was conducted by placing the devices on a bicep (Figure 4b). Similar variations in oxygenated conditions before and after venous occlusion were obtained using a commercial oximeter and a wireless epidermal device, as shown in Figure 4c. In addition to oximeter applications, they also demonstrated UV dosimetry and a skin spectrometer containing UV-responsive dyes sandwiched between PDs and LEDs in four different colors (i.e., IR, red, orange, and yellow). Although they successfully demonstrated that an expanded functional device can detect UV-dose dynamics and jaundice, further improvements, such as device miniaturization and flexibility, are required for practical application in human-compatible biomedical electronic devices.

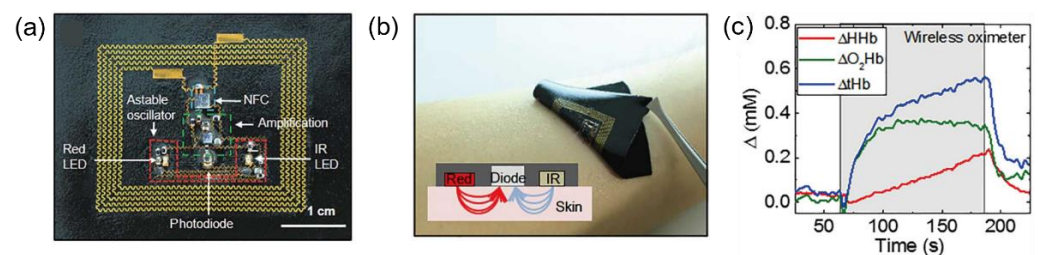


Figure 4. (a) Image of the device that includes near-field communication (NFC), amplification, a stable oscillator, two LEDs, and a photodiode on a flexible substrate (black space). (b) Photograph of the device used on the forearm. The inset shows the image of the diode receiving light in the reflective mode. (c) Measurements obtained by an epidermal device recorded from adjacent regions of the forearm. The gray area shows changes in oxyhemoglobin and deoxyhemoglobin concentrations when vein occlusion for 120 s ($\Delta\text{tHb} = \Delta\text{O}_2\text{Hb} + \Delta\text{HHb}$). Adapted with permission from [30] AAAS, 2019.

For more precise control and accurate data acquisition with a miniaturized device architecture, they improved the inductance and electronic system by using a millimeter-scale stacked loop Cu antenna with a stable microcontroller instead of multivibrator circuits (Figure 5a) [31]. The integrated devices, including the NFC chip, were fabricated in a system with a diameter of approximately 10 mm, thickness of approximately 0.9 mm, and bending radius of 3 mm. The total weight and area size are 90% less than the previously reported device architecture. This device can transmit data over a 10 cm distance using

a high-power, large-transmission antenna. Owing to their miniaturized form factor, the fabricated devices can be mounted on a fingernail or earlobe (Figure 5b). Stable extraction with minimized distortion of SpO₂ values was observed during movement, which is an important advantage of device miniaturization compared to the present commercial oximeter devices, as shown in Figure 5c. The long-term operation for 3 months without the risk of irritation, discomfort, and device performance degradation was effective, allowing for practical application in clinical treatment and human skin-compatible healthcare platforms.



Figure 5. (a) Illustration of the various constituent layers of the NFC-enabled pulse oximeter device. (b) Photograph image of measurement setup to evaluate SpO₂ level from the fingernail (up). It is possible in application of a device with a computer mouse functioning as a wireless interface. Photograph image of measurement setup to evaluate SpO₂ level from the earlobe (down). (c) Calculated SpO₂ during rest and movement on the device. The device quantified the accelerometer's signal according to the movement in the X(red), Y(blue), and Z(green) axes. Adapted with permission from [31], Wiley, 2016.

Although most Si-based PPG sensors with innovative functionalities proved to operate properly on human skin, they still inadequately conform to the skin surface owing to the intrinsic brittleness of light-responsive Si materials and the rigidity of the device structure. Li et al. proposed a thinner device architecture including LEDs and PDs [32]. The thickness of the active device components (LEDs and PD) is adjusted below 20 μm using the nanodiamond thinning process. Based on the stamp-assisted transfer printing technique, LEDs and PDs are transferred onto Au interconnects. Finally, the interconnected devices are encapsulated in 500 μm -thick polydimethylsiloxane (PDMS) and polyurethane (PU) film (Figure 6a). Under mechanical deformation, it is demonstrated that the external elastomers absorb all stresses, and strains are barely applied to the active device parts, resulting in stable device operation under a high tensile strain of 35%. Owing to their low flexural rigidity, epidermal optoelectronic devices were positioned on the wrist (Figure 6b) and forefinger (Figure 6c) and detected precise and accurate vital parameters during movement (Figure 6d). While stretching, a disturbing error occurs in the allowable range of 0.1% of the SpO₂ level. The all-inclusive device achieved by the thinning process is universal for various types of inorganic semiconducting materials, opening possibilities to fabricate skin-like functional electronic patches that can be directly mounted on human skin.

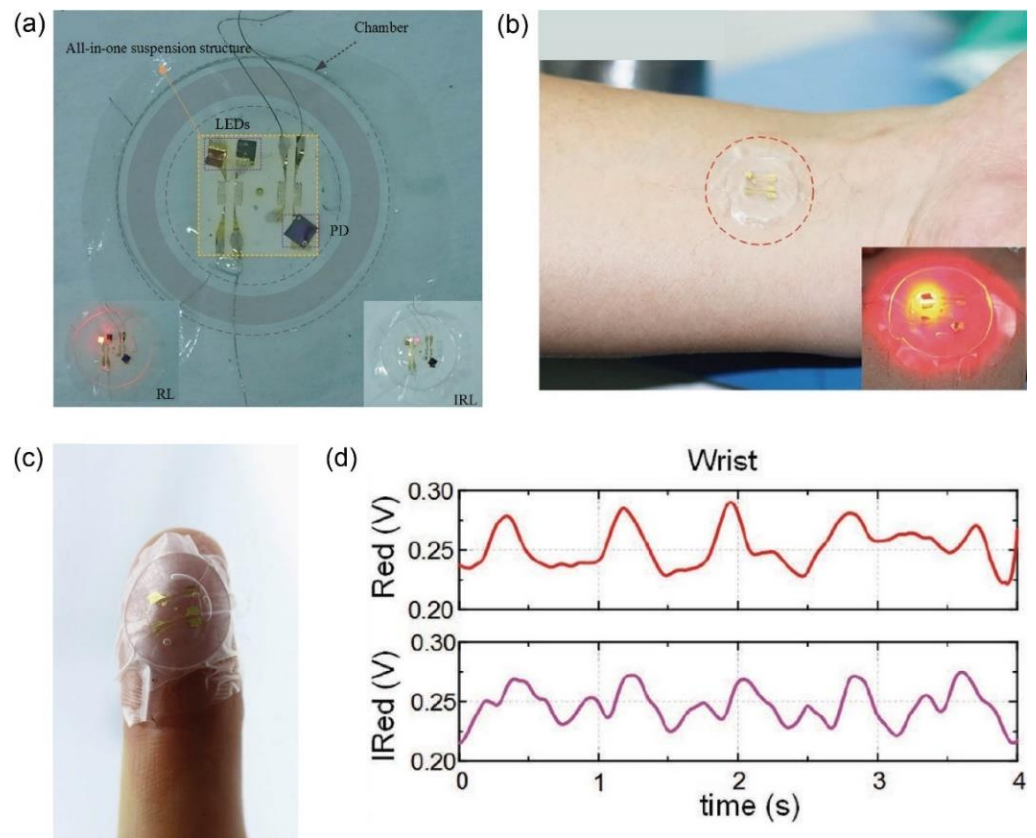


Figure 6. (a) Image of the PPG device based on GaAs and silicone material, including two LEDs and a photodetector. Inset, the left light is red (620 nm) and the right light is infrared (850 nm). (b) The image of device attached to the wrist and (c) The inset shows the stable operation of the device on fingertip. (d) The measured PPG signal while the subject's forearm moves slowly is applicable for SpO₂ calculation. Adapted with permission from [32], Wiley, 2017.

4.2. Other Inorganic Photodiodes

The GaAs is among the most frequently used III-V semiconductor materials. Kim et al. [33] reported an attachable and flexible pulse sensor composed of four inorganic GaAs photodetectors (IPDs) and two red light-emitting diodes (LEDs). To fabricate a skin-attachable pulse sensor, a mesa-etched [83] GaAs active layer on a sacrificial layer was transfer-printed onto a 12.5 μm -thick PI film substrate with 2 μm -thick SU-8 encapsulation. The devices were fully encapsulated with a polydimethylsiloxane (PDMS, 50 μm thick) layer to maintain operational stability under mechanical strain, and an additional layer of sticky silicone elastomer (Ecoflex, 20 μm thick) covered the bottom and top of the sensor for skin adhesion, as shown in Figure 7a. The completed pulse sensor can be attached to the skin with 0.3 N/cm² shear adhesion force, indicating a strong adhesion between the skin and inorganic pulse sensors with motion artifacts being minimized during device operation on the skin. The LEDs were placed next to the IPD in the same plane to measure the PPG signal in reflection mode (Figure 7b). Therefore, it could be located on the skin and/or body surfaces, such as a fingernail, fingertip, middle finger, and even a thick forearm. Although the amplitudes of the systolic and diastolic PPG signals were different depending on the device location (fingertip: 36.0 mVp-p, forearm: 2.61 mVp-p) due to the depth of the arterial vessel beneath the skin surface, it was confirmed that the standard and a clear waveform were obtained compared to those waveforms from a conventional rigid PPG sensor. Owing to the strong adhesion to the skin surface, the developed sensors could be adjusted to test HRV for running subjects (Figure 7c). After the experiments, the change in heart rates from resting to post-running was well captured, but the devices exhibited distorted waveforms after exercise due to motion artifacts caused by the external wiring.

In addition to wireless data acquisition platforms, the thickness (200 μm) of LEDs should be minimized for further flexibility improvements.

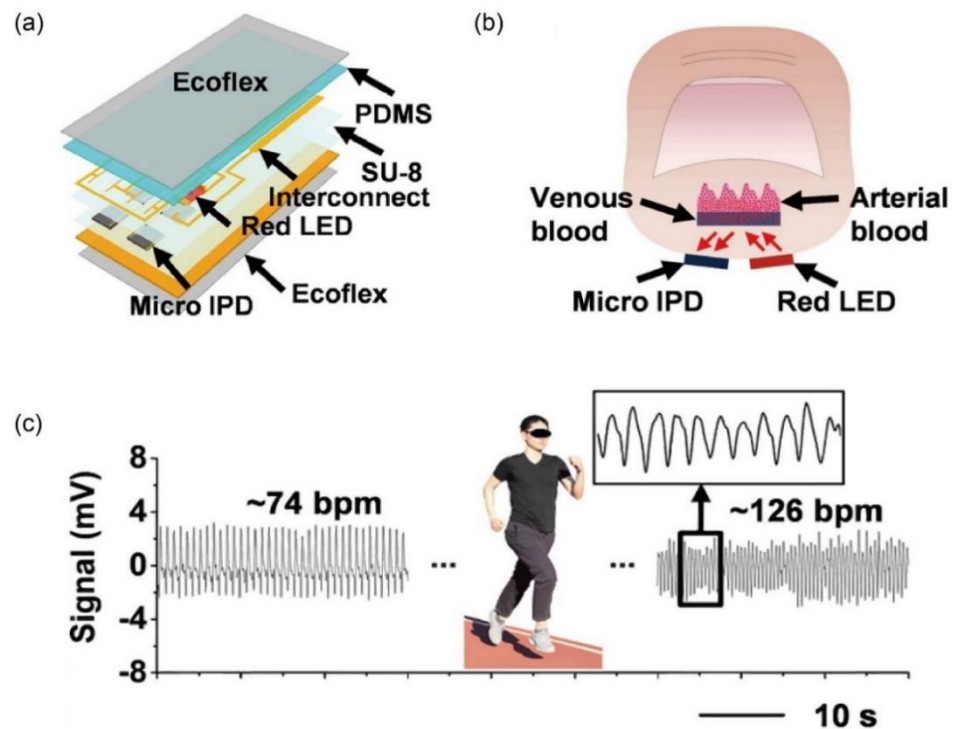


Figure 7. (a) Illustration of the attachable pulse sensor. The microsized inorganic photodetectors (IPDs; size: $760 \times 760 \mu\text{m}$) built on a GaAs substrate are fabricated on a polyimide film (PI; $\sim 12.5 \mu\text{m}$) with the support of an adhesive layer (SU-8; thickness: $\sim 2 \mu\text{m}$). The device was encapsulated with an Ecoflex layer (thickness: $\sim 300 \mu\text{m}$). (b) Schematic diagram of the principle of a pulse sensor utilizing reflection mode using IPD and LED. The LED light is reflected by blood and tissue, and the IPD receives the reflected light. (c) The PPG signal was used to measure the heart rate before and after exercise in the forearm. The heart rate during the rest period was ~ 74 bpm and the heart rate after exercise was ~ 126 bpm. Adapted with permission from [33], ACS Publications, 2017.

Quantum dots are an emerging material suitable for optoelectronic biomedical applications, including optogenetics, blood oximetry, and drug delivery [84,85]. The tunability of optical and electronic performance is shown by the nanoscale control of particle sizes.

Kim et al. [34] suggested a stretchable PbS quantum dot (QD)-based photoelectric sensor with a buckling structure. A colloidal QD was embedded as an active layer on an elastic substrate, and the full device structure of the PbS QD photodetector was displayed, as shown in Figure 8a. For elasticity, the devices are initially fabricated on PEN substrates and peeled away to be transferred onto the elastomeric substrates. The PbS-based PDs are sensitive in the range of the visible and IR spectra (400–1100 nm) with light responsivity of external quantum efficiency (EQE) of 12% at a wavelength of 618 nm. Owing to the sticky and stretchable characteristics of the devices (Figure 8b), they could adhere tightly to the skin and nail surface. Not only PDs but also stretchable QD-LEDs are demonstrated in the same manner. The operational stability in the stretching test was secured under a mechanical strain of 40% for PDs and 70% for LEDs. Finally, skin-mounted PPG sensors composed of QD-LEDs and QD-PDs were demonstrated by wrapping them around the tip of a forefinger, as shown in Figure 8c. As the patch-type devices can be mounted firmly on the skin, stable and accurate waveforms caused by a cardio-ventricular contraction can be obtained, compared to tong-type PPG sensors without motion artifacts (Figure 8d). The patch-type PbS QD-based real-time biomedical electronic devices were successfully demonstrated. Given their harmfulness, the use of heavy metals in the application of skin-compatible sensors is rejected or proper passivation layers preferentially should be

developed. In addition, stronger light responsivity and thinner device architectures are required for further development.

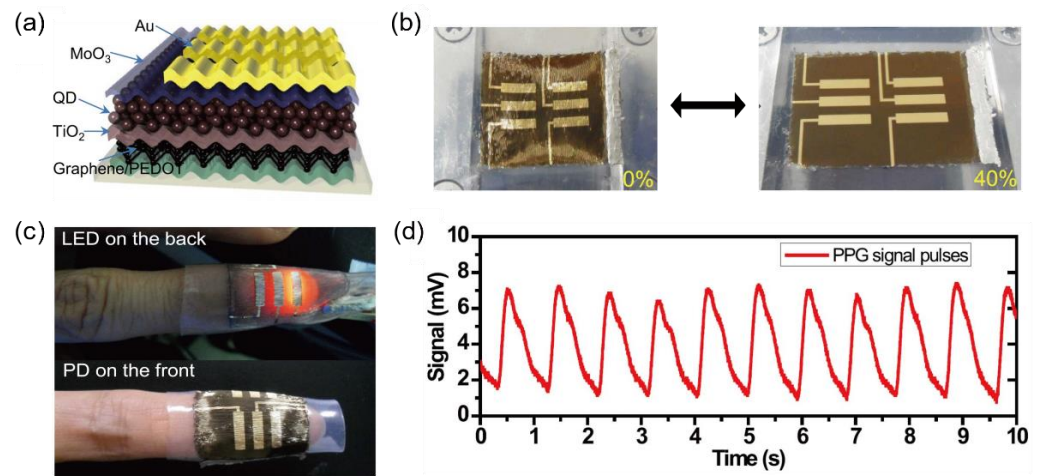


Figure 8. (a) Cross-sectional view of structure of the stretchable PbS QD photodetector excluding the elastomer substrate. (b) Optical image of the stretchable QD photodetector from 0% to 40% strain. (c) Image of working QD-LED and QD photodiode on the fingertip. (d) Records PPG pulses collected in real time under red QD-LED conditions. Adapted with permission from [34], ACS Publications, 2017.

As a photoresponsive material, graphene offers a fast response owing to efficient optical carrier separation [86], enabling various types of optoelectronic applications. Polat and co-workers [35] reported a transparent and flexible PPG sensor using graphene quantum dot (GQD) PDs. For the fabrication of skin-compatible PPG sensors, CVD-grown graphene on copper was transferred onto PEN substrates, and photoresponsive colloidal QD layers were deposited on the graphene layer (Figure 9a). In particular, GQD PDs have key features, such as broadband (300–2000 nm) wavelength sensitivity. The generated electron–hole pairs in the QD layer are separated and rapidly transferred into each layer by the graphene-QD built-in electric field. Charged carriers (holes) are trapped in the QD layer, and other separated carriers (electrons) migrate to the graphene. This leads to a measurable change in photoconductivity; thus, the responsiveness of these GQD PDs shows a high value of photoconductive gain, approximately 10^5 A/W. Their broader wavelength sensitivity allows the health patch to be operated in transmission mode even under ambient light owing to the deeper skin penetration of longer-wavelength light. Consequently, the integrated wearable device can continuously detect biometric signals over a long period with very low power consumption (140 μ W, 16 μ W on standby) (Figure 9b,c). For wireless applications, the GQD PDs were integrated with a printed circuit board (PCB), operating battery-free and with wireless data transmission using a smartphone. The noninvasive and skin-compatible GQD PDs can accurately measure vital signals on fingers, the forehead, feet, and chest with an improved degree of design freedom owing to the wide detection range of light.

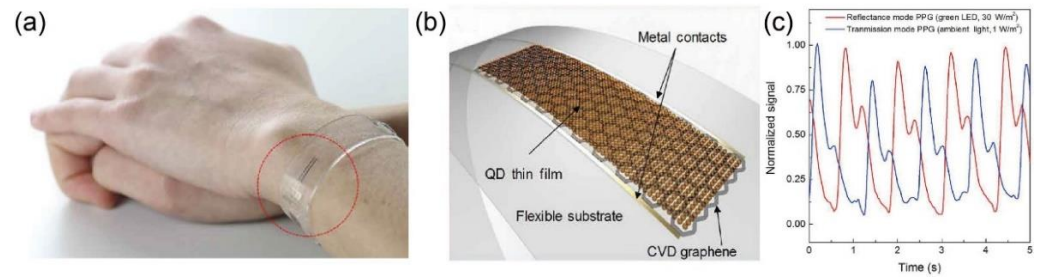


Figure 9. (a) Photograph of the flexible and transparent GQD PD attached to a bracelet-shaped wrist that can monitor heart rate. (b) Schematic illustration of the assembly of graphene and QDs on a flexible substrate. (c) Normalized PPG signal when the PPG sensor operates in transmission and reflection modes. With the high sensitivity and mechanical flexibility of the GQD PD, the health patch can operate accurately for long periods in transmission and reflection modes. Adapted with permission from [35], AAAS, 2019.

4.3. Organic Photodiodes

PPG sensors using organic materials have attracted much attention owing to their multiple advantages, such as high flexibility, easy processing, low fabrication cost, and large fabrication volume. Lochner and coworkers reported a flexible PPG sensor consisting of organic absorbers responsive to green (532 nm) and red (626 nm) light [49]. The key technology uses an organic layer responsive to green wavelengths, instead of near-infrared wavelengths (800–1000 nm), as the difference in the light absorption properties of oxygenated and deoxygenated hemoglobin is similar in both wavelength regions. The bulk-heterojunction (BHJ) is composed of poly([4,8-bis[(2-ethylhexyl)oxy]benzo[1,2-b:4,5-b']dithiophene-2,6-diyl]{3-fluoro-2-[(2-ethylhexyl) carbonyl] thieno[3,4-b]thiophenediyl}) (PTB7) and PC71BM as the donor: acceptor system. The fabricated organic photodetectors (OPDs) exhibit EQE of 38% and 47%, respectively, at 532 and 626 nm with a leakage current of approximately 1 nA cm^{-2} at 2 V applied with reverse bias. Figure 9c shows the acquired PPG signals using all-organic optoelectronic sensors composed of rigid OLEDs and flexible OPDs. Although the magnitude of signals is reduced compared to conventional inorganic devices, it was sufficient to resolve the PPG waveforms and calculate blood oxygenation levels in arterial blood with an error of 1% for heart rate and 2% for oxygen saturation. It is suggested that flexible wearable devices using organic materials have potential applications as medical devices owing to their large area scalability and flexibility. For more skin conformability, the rigidity of devices should be further reduced by controlling the overall device thickness and by designing compatible device architectures.

Yokota and coworkers [36] developed ultra-flexible three-color (i.e., red, green, and blue) polymer light-emitting diodes (PLEDs) with the integration of organic photodetectors (OPDs) in the application of PPG sensors (Figure 10a). For a skin-compatible design, the devices were fabricated on an ultra-thin substrate composed of 1 μm -thick parylene as the supporting layer and 500 nm-thick polyimide as the planarization layer on the glass substrate. After being peeled from the glass substrate, the total thickness of the PLEDs and OPDs is less than 3 μm , which is thinner than the epidermal layer of human skin. Therefore, the device could be flexible with a bending radius of 100 μm owing to the thin form factor and low stiffness, while the device's operation under mechanical deformation is negligibly affected as the active component is located at the neutral plane. As shown in Figure 10b,c, each PLED exhibits remarkable color expression with high EQE and luminance as high as 13.9% and 4900 cd/m^2 (for green PLED, $\lambda_{\text{peak}} = 517 \text{ nm}$) and operational stability under repetitive mechanical deformation. In addition to PLEDs, OPDs with an active layer of poly(3-hexylthiophene)(P3HT):(6,6)-phenyl-C61-butyric acid methyl ester (PCBM) exhibit prominent spectral responsivity corresponding to the electroluminescence spectra of the fabricated PLEDs. The PLEDs and OPD were integrated to create a skin-compatible pulse oximeter. The devices were wrapped over a finger to measure pulse and blood oxygen levels in reflective mode, as shown in Figure 10d. By changing the oxygen saturation

from 99% to 90%, the amplitude of the light-responsive signal from the green PLED was observed to have decreased more than that of the red PLED (Figure 10e), indicating good agreement with previously reported results using organic oximeters on glass and thick plastic substrates [49].

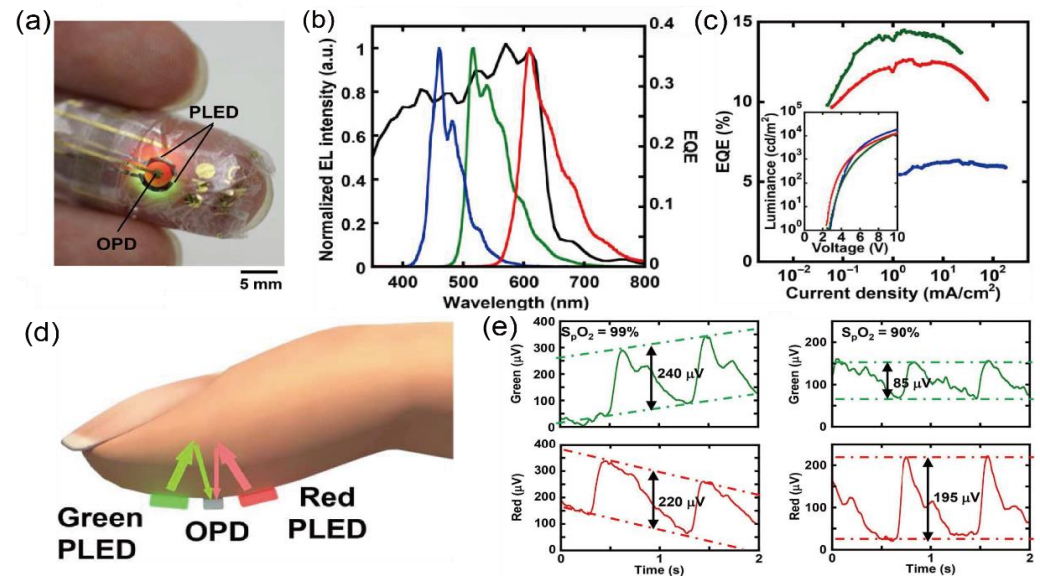


Figure 10. (a) Image of an ultra-flexible organic device used on the finger. (b) External quantum efficiency (EQE) of organic photodetector (OPD) (black line) according to the wavelength of light with polymer light-emitting diode (PLED) blue (blue line), green (green line), and red (red line). (c) Current density and EQE correlation characteristics in ultra-flexible PLED. (d) Working principle of the reflection mode pulse oximeter on the finger. (e) Output signal of OPD obtained using the ratio of oxyhemoglobin in blood. The green and red lines signify signals when the green and red PLEDs work, respectively. The left figure is the signal when SpO_2 is 99%, and the right figure is the signal when SpO_2 is 90%. Adapted with permission from, [36] AAAS, 2016.

Organic PPG sensors simultaneously targeting mechanical conformability and fast responsivity in the near-infrared (IR) region are a prerequisite for expanding the capabilities for skin-mounted applications. Park et al. reported an ultra-flexible skin conformal PPG sensor (Figure 11a) [37], utilizing a BHJ active layer of a polyindacenodithiophene-pyridyl-[1–3]thiadiazole-cyclopentadithiophene (PIP3CP) polymer as an acceptor (Figure 11b) and PC61BM as the donor, respectively. They were built on an ultra-thin (1 μm -thick) parylene substrate with an inverted structure, and the devices were located in the neutral plane within 3 μm of the overall device thickness, resulting in high skin-conformability between the ultra-flexible device and the skin surface (Figure 11c). The OPDs exhibit high response speed (>1 kHz) due to the favorable self-organization of the regioregular polymer chains. The implemented PPG sensor exhibited high on/off switching characteristics and excellent skin compatibility characteristics. As the devices were in neutral positions, the near-infrared responsivity was maintained under extremely deformed conditions. The invariant V_{OC} , FF, and normalized J_{SC} values under 20–200% tensile strain indicate that the BHJ maintained its charge collection, transporting, and collection behavior under mechanical deformation. Using an OPD with a commercial rigid near-infrared (NIR) LED, they demonstrated that the ultra-thin organic photodetector can detect consistent and repetitive cardiovascular signals under the illumination of near-infrared (800 nm) light, which is comparable to the sensitivity of the glass references (Figure 11d). In addition, Fourier analysis in the frequency domain in Figure 11e indicates a representative heart rate (i.e., 64 BPM) in the acceptable range for an adult. Thus, additional work on the integration of highly flexible near-infrared organic LEDs and OPDs will allow the practical implementation of all organic-based conformal

PPG sensors. As a proof-of-concept for a portable cardiovascular sensor, fast responsiveness and mechanical conformability should be balanced for skin-conformable electronics.

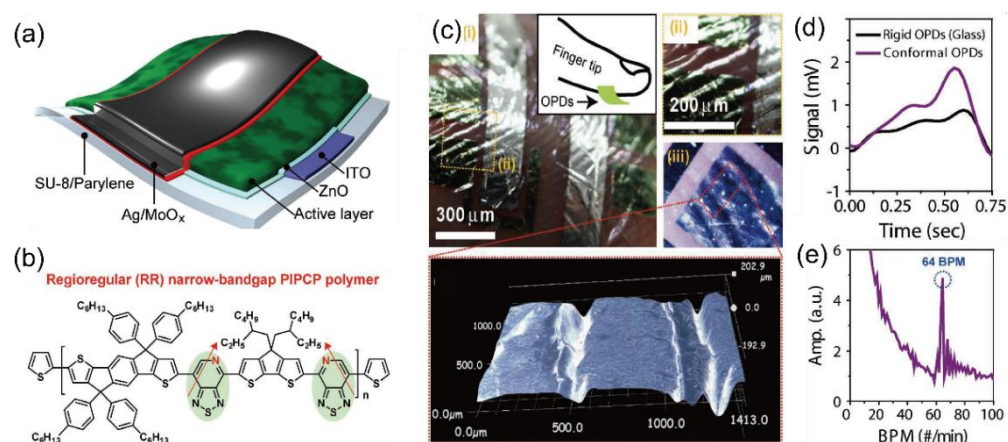


Figure 11. (a) Schematic device structure of the near-IR photoresponsive ultra-flexible organic photodetector. The devices are fabricated on polymeric substrates. After fabrication, the devices are passivated with a 1 μm -thick parylene layer. (b) Chemical structure of PIPCP. The regioregularity of the PIPCP polymer is highlighted with a red arrow, indicating the orientation of asymmetric pyridyl-[1-3]thiadiazole (PT) unit. (c) (i, left top image) Photograph of fingerprint-conformal near-IR photodetectors and inset indicates the position of the skin-conformal near-IR photodetector on the finger (ii, right top image) enlarged image of (i), and (iii, right bottom image) microscope image of top silver electrode and skin surface, indicating high skin-conformability. (bottom) 3D microscope image of ultra-flexible near-IR organic detectors on the surface of a human index fingertip. (d) Comparison of the output signal between the glass reference (black) and the skin-conformal near-IR photoplethysmogram sensor (purple) wrapped over a fingertip with a 99% blood oxygenation level. (e) Beats per minute (BPM) analyzed from measured output signals using fast Fourier transform (FFT) signal processing (64 BPM is the representative heart rate in the acceptable range for adults aged 15–30 years). Adapted with permission from [37], Wiley, 2018.

In addition to the development of unit device performance measuring the oxygenation level of a single spot in the transmission mode, two-dimensional (2D) mapping of vital conditions based on the reflectance mode enables the spatial monitoring of tissue and organ wounds. Khan et al. [38] reported the reflectance oximeter array (ROA), a flexible organic electronic system realized by printing, and its integration with silicon circuits for oximetry. They fabricated the ROA with eight OPDs and eight OLEDs that irradiate near-infrared (725 nm) and red (612 nm) wavelengths of light (Figure 12a). ROA is made by stacking OPD and OLED arrays made on separate substrates. The OPD array consists of eight OPD pixels, rows 1 and 3 contain the four red OLED pixels, and rows 2 and 4 contain the four NIR OLED pixels. Using a flexible flat cable, the printed ROA was connected to the control electronic board. With an additional circuit of the analog front end (AFE), OPDs can read the PPG signals corresponding to sequentially operated red and NIR OLEDs (Figure 12b). The fabricated ROA was tested to monitor oxygen saturation in the foreheads (Figure 12c) and forearms (Figure 12d) of human volunteers under varying oxygen concentrations. It was revealed that a mean error rate of 1.1% was confirmed compared to a commercial finger probe. After collecting data from all nine pixels, 2D contour maps of PPG signals from red and NIR OLEDs and changes in oxygen saturation level are created (Figure 12e). Through the 2D-mapping function, the ROA can provide the spatial oxygen saturation level and can be adopted to monitor the oxygen supply in tissue, wounds, and newly transplanted organs. Their proposed ROA device can be placed in various locations beyond those used for conventional sensing and is expected to be used in medical detection applications, such as real-time chronic health monitoring and post-operative recovery management.

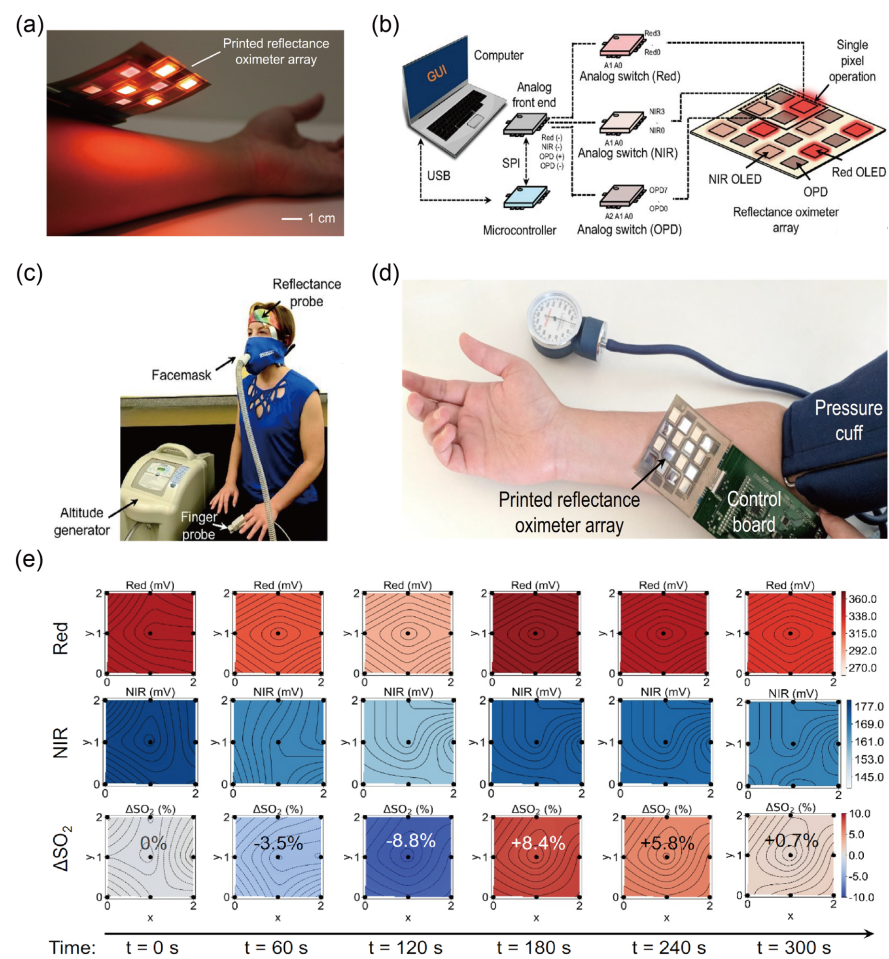


Figure 12. (a) Image of the reflectance oximeter array (ROA) applied to the human forearm. (b) Schematic of the reflectance oximeter system. (c) Setup for changing the human subject's oxygen saturation. The subject breathes through a face mask, and the oxygen content is changed using an altitude simulator. SpO₂ was measured with a conventional probe on the finger and a reflectance oximeter on the forehead. (d) Setup to measure oxygen saturation changes in the forearm using ROA. The pressure cuff controls the blood supply to the forearm. The ROA provides 3 × 3 oximeter pixels in a 4 × 4 device. (e) Two-dimensional contour maps showing red, NIR, and ΔSO₂; normal condition (t = 0 s), ischemia condition (t = 60, 120 s), and after releasing the pressure cuff (t = 180, 240, 300 s). Adapted with permission from [38], AAAS, 2016.

For accurate vital signal measurement, a high signal-to-noise (SNR) ratio should be determined. The deliberate design of PPG devices could encourage the development of highly sensitive skin-compatible PPG sensors. Khan and coworkers [39] studied wearable PPG sensors in reflection mode by careful consideration of sensor geometry, such as shape, spacing, and optical barriers. They explored three sensor geometries, namely, a rectangular shape, a bracket shape, and a circular geometric shape (Figure 13a–d) with optical barriers to minimize light scattering (Figure 13e,f). As a reference device, the rectangular shape exhibited a low SNR value, as the OLED does not surround the OPD. Therefore, new bracket and circular geometry designs with reduced distances between the light-emitting and responsive devices were proposed to minimize the loss of reflected light. The bracket and circular designs enhance the magnitude of the PPG signal, resulting in the improvement of SNR values. The proposed geometry improved by as much as 48.6% in the red channel and 18.2% in the NIR channel, compared to the rectangular geometry. In addition, optical barriers were used to minimize light scattering between the OLED and OPD (Figure 13f). Based on the results of the geometry study, the developed PPG sensors with the new architecture were applied on the wrist at different locations (Figure 13g). For

multichannel data acquisition, motion artifacts (MA) should be reduced to evaluate the heart rate (HR) and pulse oximetry results. By implementing two algorithms, template matching (TM) and inverse variance weight (IVW) with an ideal PPG signal, the HR and oximetry data were accurately evaluated. The pulsating PPG signal above the wrist was the weakest, while the ulnar and radial artery provided the clearest PPG signal, as shown in Figure 13h. The study suggested that the proper design of the effective area, the spacing between the light emission and detection devices, and proper adjustment of optical barriers to minimize light scattering could improve the SNR values. The use of inverse-variance weighting and a template matching algorithm could also improve the accurate detection of vital signals.

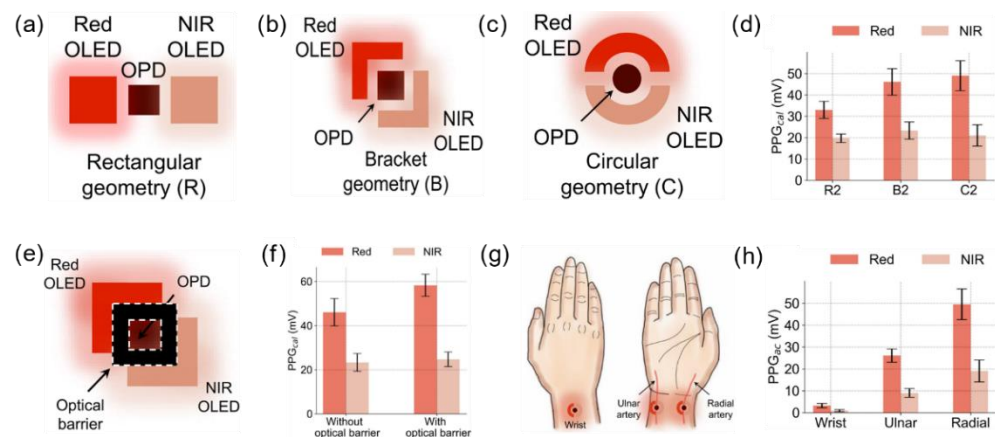


Figure 13. (a) Two LEDs are arranged on both sides of the OPD in a rectangular geometry, (b) in the geometry of brackets, and (c) in a circular geometry. (d) PPG signal magnitudes depending on LED and OPD shape conditions. In R2 (rectangular), B2 (brackets), and C2 (circular), 2 implies the distance between the emitter and detector is 2 mm. Red bars represent the data for red LEDs and peach-colored bars represent data for NIR LEDs. The error bars are represented by data obtained after three repeated experiments. (e) Illustration of an oximeter sensor in reflection mode with an optical barrier (black space) in the space between the emitter and detector. (f) The PPG signal magnitudes with or without an optical barrier in the red and NIR channels. The error bars are represented by data obtained after three repeated experiments. (g) Figure showing the three locations where the sensor is placed: on top of the wrist, ulnar artery, and radial artery. (h) The magnitude of the PPG signal measured in the wrist, ulnar, and radial arteries. The error bars are represented by data obtained after three repeated experiments. Adapted with permission from [39], IEEE, 2019.

Its high-power consumption makes it difficult to use as a standalone continuous monitoring system that can be integrated easily into everyday life. A low-power-consuming health monitoring system that can be worn all day in real-time would help in the diagnosis and prognosis of cardiovascular diseases. Xu et al. [40] reported on epidermal and flexible near-infrared (NIR) PPG sensors by combining low-power, high-sensitivity organic phototransistors (OPTs), and high-efficiency inorganic light-emitting diodes. NIR has the advantage of having deeper penetration into the skin due to low light attenuation. Therefore, larger pulsatile PPG signals can be collected from arterioles in the deeper layers of the skin. In this study, they demonstrated skin-compatible NIR-responsive OPTs (Figure 14a–c). For device fabrication, a 1.8 μm -thick polyimide (PI) layer is formed on the Si wafer by spin-coating and acts as a polymeric thin substrate after delamination from the silicon wafer. It is noted that a bilayer of $\text{SiO}_2/\text{Al}_2\text{O}_3$ was utilized to achieve a low voltage (<3 V) device operation. SiO_2 is sputtered over the Al_2O_3 layer to form a better interface profile on the surface. The devices were finally encapsulated with 200 nm-thick polytetrafluoroethylene (PTFE) and 1.6 μm -thick parylene C as a sufficient barrier to the diffusion of oxygen and water molecules in direct contact with human skin. In conclusion, they designed a bandage-shaped, NIR responsive epidermal Hybrid PPG

(hPPG) sensor composed of an OPT and LED by embedding in 300 μm -thick Polydimethylsiloxane (PDMS) with a thin ($\approx 25 \mu\text{m}$) elastic acrylic adhesive to the skin (Figure 14d). It was observed that the mean values of systolic blood pressure (SBP) and diastolic blood pressure (DBP) were consistent with those obtained from the conventional rigid type PPG sensor (cPPG)/ECG setup. This study suggests that low-power hybrid PPG sensors have a benefit in the diagnosis and prognosis of cardiovascular diseases for real-time and portable physiological monitoring systems.

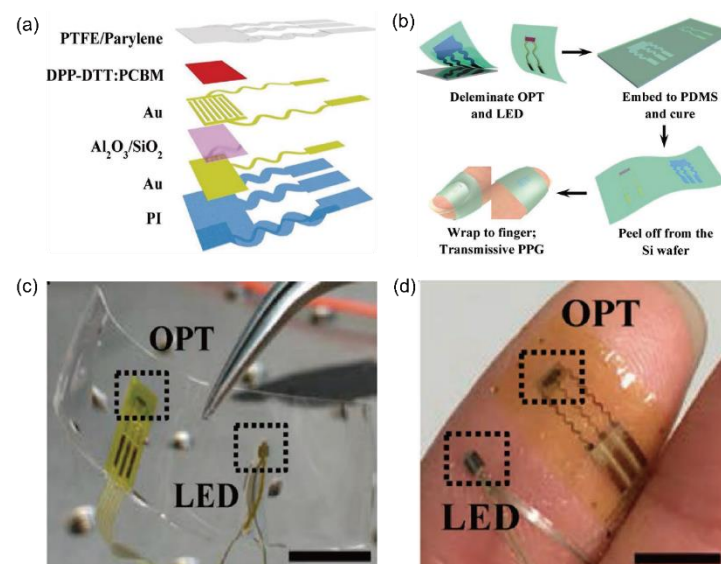


Figure 14. (a) Schematic of the device structure of the flexible NIR organic phototransistor (OPT). (b) Process diagram of fabricating a flexible hPPG sensor and applying to the finger. (c) The image of the flexible sensor in the peel-off state during the process. (d) Image of a finger attached with the epidermal NIR hybrid PPG (hPPG) sensor (scale bar, 5 mm). Adapted with permission from [40], Wiley, 2017.

Lee et al. [41] proposed a patch-type organic pulse oximeter (OPO) sensor with very low power consumption based on flexible OLEDs and OPDs. The device structure and materials of the green and red OLEDs with OPDs for the proposed OPO sensor are presented in Figure 15a. The peripheral oxygen saturation (SpO₂) measurements require two spectral light sources (i.e., green and red). Therefore, OPDs are composed of 4,4'-cyclohexylidenebis [N, N-bis (4-methylphenyl) benzenamine] (TAPC) and C70 of the mixed layer as an active component. The light absorption of OPDs occurs in all directions with a surrounding structure resembling the number 8, indicating reduced light wastage (Figure 15b). In a reflective measurement mode, the completed OPO sensors can be applied to various body parts, such as the finger, wrist, neck, and nose, and operate properly (Figure 15c). The power consumption of the green and red OLEDs was as low as 31 and 17 μW , respectively. It is noted that the developed device has the lowest power usage, including OLED- and LED-based sensors with the same duty ratio, compared to previous reports (Figure 15d). The study demonstrates the potential of a low-power health-monitoring system that could be operated throughout the day with form factor benefits from using organic materials.

As growing attention for wearable sensor platforms, textile-based sensors are of great significance to skin-compatible electronics. Kim et al. [42] fabricated highly efficient OPDs on fiber (fOPD) using spirally-wrapped carbon nanotubes (CNT) as microelectrodes (Figure 16a). The feasibility of bandage-type fOPD was tested by incorporating red (638 nm) and green (525 nm) LEDs (Figure 16b). The repetitive systolic and diastolic peaks were observed in reflection and transmission modes with the same period (Figure 16c). The fab-

ricated fOPD can maintain 80% of the electrical performance when it is bent with a bending radius of 1.75 mm, which shows the prospect of the fiber-based optoelectronic devices.

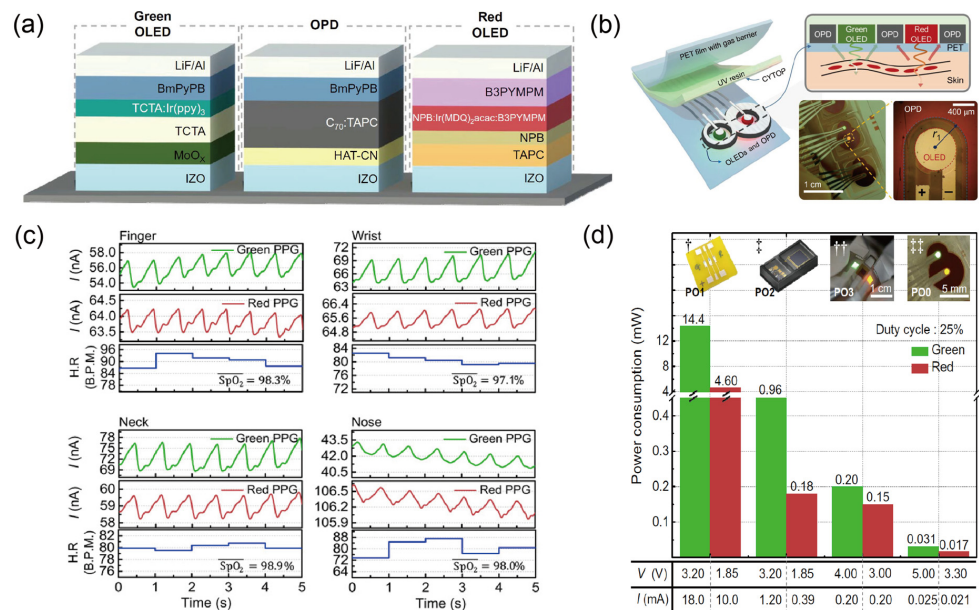


Figure 15. (a) Sectional view of green OLED, OPD, and red OLED in a complete OPO sensor. (b) Image of the proposed OPO sensor with an enlarged cross-sectional view to depict the device arrangement and light-receiving process through the skin. The picture of an OPO sensor in operation is also shown. Note that the Figure 8-shaped OPD wraps around red and green OLEDs in operation. (c) PPG signals, SpO₂ values, and heart rate obtained from various body parts. (d) Comparison of the power consumption of R and G light sources of oximetry sensors: †, discrete optical elements integrated on a PCB substrate with the edge-to-edge distance between elements being 2 mm (=PO1); ‡, a commercially available reflective pulse oximetry head (SFH7050, Osram Sylvania Inc.) (=PO2); ††, OPO sensor wherein rectangular OLEDs and OPDs are arranged side by side with an edge-to-edge distance of 2 mm (=PO3); †††, the OPO sensor proposed in this work (=PO0). The layer configurations of OLEDs and OPD in the OPO sensor used in †† are identical to those used in this work. Adapted with permission from [41], AAAS, 2018.

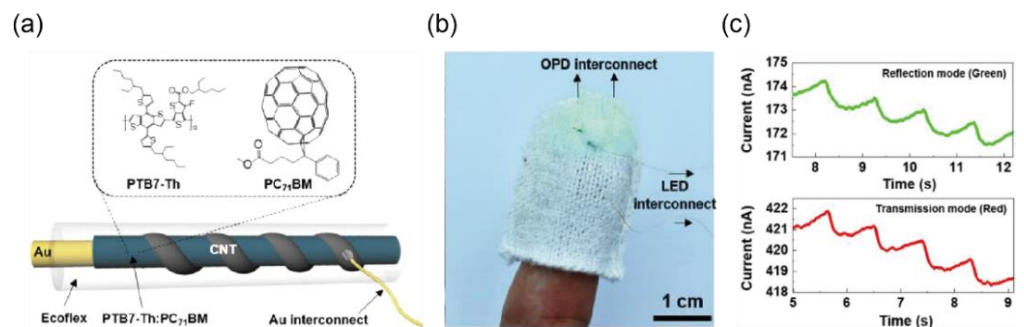


Figure 16. (a) Schematic of the device structure fOPD and the chemical structures of the materials used. (b) Photographs of fOPD integrated into a medical bandage with red and green LEDs for PPG sensing. (c) PPG signals measured from the fOPD in reflection and transmission modes. Adapted with permission from [42], ACS Publications, 2020.

5. Conclusions

The skin-compatible PPG sensors have enabled significant advances in biomedical and health self-care platforms. In this paper, various types of skin-compatible PPG sensors were systematically studied. Different types of semiconducting materials, device architectures, designs, and strategies for securing skin compatibility with high SNR values

were highlighted. However, challenges for future practical applications remain. From the device performance perspective, accurate and stable PPG signals without motion artifacts should be obtained. Therefore, the mechanical durability and skin conformability of skin-compatible detectors are necessary without compromising electrical performance. In addition to the accurate signal acquisition, the introduction of array structures with a systematic algorithm for the raw signal calculation can help in the exact evaluation of human body conditions. For further studies, the detection of specific information with significant hemoglobin derivatives can provide early notice of exposure to specific drugs or environmental toxins with a suitable photodetector measuring at various wavelengths. We believe that real-time healthcare monitoring systems that are compatible with human skin will be helpful in research and development through innovative ideas in current wearable PPG sensors.

Author Contributions: I.L., N.P., and S.P. conceived the review; I.L., N.P., J.H.K., and S.P. wrote the manuscript; H.L. and C.H. revised the manuscript. All authors have read and agreed to the published version of the manuscript.

Funding: National Research Foundation of Korea: NRF-2020R1F1A1073564; Ministry of Food and Drug Safety: Program No. 21153-431; National Research Foundation of Korea: 2009-0082580.

Institutional Review Board Statement: Not applicable.

Informed Consent Statement: Not applicable.

Data Availability Statement: Not applicable.

Conflicts of Interest: The authors declare no conflict of interest.

References

1. Ghamari, M. A Review on Wearable Photoplethysmography Sensors and Their Potential Future Applications in Health Care. *Int. J. Biosens. Bioelectron.* **2018**, *4*, 195–202. [[CrossRef](#)] [[PubMed](#)]
2. Rawassizadeh, R.; Price, B.A.; Petre, M. Wearables: Has the Age of Smartwatches Finally Arrived? *Commun. ACM* **2014**, *58*, 45–47. [[CrossRef](#)]
3. Wei, J. How Wearables Intersect with the Cloud and the Internet of Things: Considerations for the Developers of Wearables. *IEEE Consum. Electron. Mag.* **2014**, *3*, 53–56. [[CrossRef](#)]
4. Riazul Islam, S.M.; Kwak, D.; Humaun Kabir, M.; Hossain, M.; Kwak, K.-S. The Internet of Things for Health Care: A Comprehensive Survey. *IEEE Access* **2015**, *3*, 678–708. [[CrossRef](#)]
5. Martins, A.F.; Santos, D.F.S.; Perkusich, A.; Almeida, H.O. UPnP and IEEE 11073: Integrating Personal Health Devices in Home Networks. In Proceedings of the 2014 IEEE 11th Consumer Communications and Networking Conference (CCNC), Las Vegas, NV, USA, 10–13 January 2014.
6. Jeong, S.; Kim, S.; Kim, D.; Youn, C.-H.; Kim, Y.-W. A Personalized Healthcare System for Chronic Disease Care in Home-Hospital Cloud Environments. In Proceedings of the 2013 International Conference on ICT Convergence (ICTC), Jeju, Korea, 14–16 October 2013; pp. 371–376.
7. Adamson, P.B.; Abraham, W.T.; Aaron, M.; Aranda, J.M.; Bourge, R.C.; Smith, A.; Stevenson, L.W.; Bauman, J.G.; Yadav, J.S. CHAMPION* Trial Rationale and Design: The Long-Term Safety and Clinical Efficacy of a Wireless Pulmonary Artery Pressure Monitoring System. *J. Card. Fail.* **2011**, *17*, 3–10. [[CrossRef](#)] [[PubMed](#)]
8. Mukhopadhyay, S.C. Wearable Sensors for Human Activity Monitoring: A Review. *IEEE Sens. J.* **2015**, *15*, 1321–1330. [[CrossRef](#)]
9. Gao, W.; Emaminejad, S.; Nyein, H.Y.Y.; Challa, S.; Chen, K.; Peck, A.; Fahad, H.M.; Ota, H.; Shiraki, H.; Kiriya, D.; et al. Fully Integrated Wearable Sensor Arrays for Multiplexed in Situ Perspiration Analysis. *Nature* **2016**, *529*, 509–514. [[CrossRef](#)] [[PubMed](#)]
10. Chan, M.; Estève, D.; Fourniols, J.-Y.; Escriba, C.; Campo, E. Smart Wearable Systems: Current Status and Future Challenges. *Artif. Intell. Med.* **2012**, *56*, 137–156. [[CrossRef](#)]
11. Yang, G.; Pang, G.; Pang, Z.; Gu, Y.; Mantysalo, M.; Yang, H. Non-Invasive Flexible and Stretchable Wearable Sensors with Nano-Based Enhancement for Chronic Disease Care. *IEEE Rev. Biomed. Eng.* **2019**, *12*, 34–71. [[CrossRef](#)]
12. Ghamari, M.; Janko, B.; Sherratt, R.; Harwin, W.; Piechockic, R.; Soltanpur, C. A Survey on Wireless Body Area Networks for EHealthcare Systems in Residential Environments. *Sensors* **2016**, *16*, 831. [[CrossRef](#)]
13. Park, S.; Jayaraman, S. Enhancing the Quality of Life through Wearable Technology. *IEEE Eng. Med. Biol. Mag.* **2003**, *22*, 41–48. [[CrossRef](#)] [[PubMed](#)]
14. Liu, Y.; Wang, H.; Zhao, W.; Zhang, M.; Qin, H.; Xie, Y. Flexible, Stretchable Sensors for Wearable Health Monitoring: Sensing Mechanisms, Materials, Fabrication Strategies and Features. *Sensors* **2018**, *18*, 645. [[CrossRef](#)]

15. Parak, J.; Korhonen, I. Evaluation of Wearable Consumer Heart Rate Monitors Based on Photoplethysmography. In Proceedings of the 2014 36th Annual International Conference of the IEEE Engineering in Medicine and Biology Society, Chicago, IL, USA, 26–30 August 2014; pp. 3670–3673.
16. McCombie, D.; Asada, H.; Reisner, A. Identification of Vascular Dynamics and Estimation of the Cardiac Output Waveform from Wearable PPG Sensors. In Proceedings of the 2005 IEEE Engineering in Medicine and Biology 27th Annual Conference, Shanghai, China, 17–18 January 2006; pp. 3490–3493.
17. Cha, J.; Choi, H.; Shin, J.; Lee, K. Unconstrained Respiration and Heart Rate Monitoring System Based on a PPG Pillow during Sleep. In Proceedings of the 2008 30th Annual International Conference of the IEEE Engineering in Medicine and Biology Society, Vancouver, BC, Canada, 20–25 August 2008; pp. 3224–3226.
18. Rozi, R.M.; Usman, S.; Ali, M.A.M.; Reaz, M.B.I. Second Derivatives of Photoplethysmography (PPG) for Estimating Vascular Aging of Atherosclerotic Patients. In Proceedings of the 2012 IEEE-EMBS Conference on Biomedical Engineering and Sciences, Langkawi, Malaysia, 17–19 December 2012.
19. Zakaria, H.; Mengko, T.L.R. Endothelial Dysfunction Assessment by Finger Photoplethysmogram. In Proceedings of the 2017 6th International Conference on Electrical Engineering and Informatics (ICEEI), Langkawi, Malaysia, 25–27 November 2017; pp. 1–4.
20. Allen, J.; Frame, J.R.; Murray, A. Microvascular Blood Flow and Skin Temperature Changes in the Fingers Following a Deep Inspiratory Gasp. *Physiol. Meas.* **2002**, *23*, 365–373. [[CrossRef](#)]
21. Servati, A.; Zou, L.; Wang, Z.; Ko, F.; Servati, P. Novel Flexible Wearable Sensor Materials and Signal Processing for Vital Sign and Human Activity Monitoring. *Sensors* **2017**, *17*, 1622. [[CrossRef](#)]
22. Slapničar, G.; Luštrek, M.; Marinko, M. Continuous Blood Pressure Estimation from PPG Signal. *Informatica* **2018**, *42*, 10.
23. Zhang, Q.; Kadefors, R. A Non-Invasive Measure of Changes in Blood flow in the Human Anterior Tibial Muscle. *Eur. J. Appl. Physiol.* **2001**, *84*, 448–452. [[CrossRef](#)] [[PubMed](#)]
24. Wu, H.-T.; Lee, C.-H.; Liu, A.-B. Assessment of Endothelial Function Using Arterial Pressure Signals. *J. Signal Process. Syst.* **2011**, *64*, 223–232. [[CrossRef](#)]
25. Matsumura, K.; Rolfe, P.; Lee, J.; Yamakoshi, T. iPhone 4s Photoplethysmography: Which Light Color Yields the Most Accurate Heart Rate and Normalized Pulse Volume Using the IPhysioMeter Application in the Presence of Motion Artifact? *PLoS ONE* **2014**, *9*, e91205. [[CrossRef](#)] [[PubMed](#)]
26. Asada, H.H.; Shaltis, P.; Reisner, A.; Rhee, S.; Hutchinson, R.C. Mobile Monitoring with Wearable Photoplethysmographic Biosensors. *IEEE Eng. Med. Biol. Mag.* **2003**, *22*, 28–40. [[CrossRef](#)]
27. Xu, S.; Zhang, Y.; Jia, L.; Mathewson, K.E.; Jang, K.-I.; Kim, J.; Fu, H.; Huang, X.; Chava, P.; Wang, R.; et al. Soft Microfluidic Assemblies of Sensors, Circuits, and Radios for the Skin. *Science* **2014**, *344*, 70–74. [[CrossRef](#)]
28. Huang, X.; Liu, Y.; Chen, K.; Shin, W.-J.; Lu, C.-J.; Kong, G.-W.; Patnaik, D.; Lee, S.-H.; Cortes, J.F.; Rogers, J.A. Stretchable, Wireless Sensors and Functional Substrates for Epidermal Characterization of Sweat. *Small* **2014**, *10*, 3083–3090. [[CrossRef](#)] [[PubMed](#)]
29. Kim, J.; Banks, A.; Cheng, H.; Xie, Z.; Xu, S.; Lee, J.W.; Liu, Z.; Gutruf, P.; Huang, X.; Wei, P.; et al. Epidermal Electronics with Advanced Capabilities in Near-Field Communication. *Small* **2015**, *11*, 906–912. [[CrossRef](#)] [[PubMed](#)]
30. Kim, J.; Salvatore, G.A.; Araki, H.; Chiarelli, A.M.; Xie, Z.; Banks, A.; Sheng, X.; Liu, Y.; Lee, J.W.; Jang, K.-I.; et al. Battery-Free, Stretchable Optoelectronic Systems for Wireless Optical Characterization of the Skin. *Sci. Adv.* **2016**, *2*, e1600418. [[CrossRef](#)] [[PubMed](#)]
31. Kim, J.; Gutruf, P.; Chiarelli, A.M.; Heo, S.Y.; Cho, K.; Xie, Z.; Banks, A.; Han, S.; Jang, K.-I.; Lee, J.W.; et al. Miniaturized Battery-Free Wireless Systems for Wearable Pulse Oximetry. *Adv. Funct. Mater.* **2017**, *27*, 1604373. [[CrossRef](#)] [[PubMed](#)]
32. Li, H.; Xu, Y.; Li, X.; Chen, Y.; Jiang, Y.; Zhang, C.; Lu, B.; Wang, J.; Ma, Y.; Chen, Y.; et al. Epidermal Inorganic Optoelectronics for Blood Oxygen Measurement. *Adv. Healthc. Mater.* **2017**, *6*, 1601013. [[CrossRef](#)] [[PubMed](#)]
33. Kim, J.; Kim, N.; Kwon, M.; Lee, J. Attachable Pulse Sensors Integrated with Inorganic Optoelectronic Devices for Monitoring Heart Rates at Various Body Locations. *ACS Appl. Mater. Interfaces* **2017**, *9*, 25700–25705. [[CrossRef](#)]
34. Kim, T.-H.; Lee, C.-S.; Kim, S.; Hur, J.; Lee, S.; Shin, K.W.; Yoon, Y.-Z.; Choi, M.K.; Yang, J.; Kim, D.-H.; et al. Fully Stretchable Optoelectronic Sensors Based on Colloidal Quantum Dots for Sensing Photoplethysmographic Signals. *ACS Nano* **2017**, *11*, 5992–6003. [[CrossRef](#)]
35. Polat, E.O.; Mercier, G.; Nikitskiy, I.; Puma, E.; Galan, T.; Gupta, S.; Montagut, M.; Piqueras, J.J.; Bouwens, M.; Durduran, T.; et al. Flexible Graphene Photodetectors for Wearable Fitness Monitoring. *Sci. Adv.* **2019**, *5*, eaaw7846. [[CrossRef](#)] [[PubMed](#)]
36. Yokota, T.; Zalar, P.; Kaltenbrunner, M.; Jinno, H.; Matsuhisa, N.; Kitanosako, H.; Tachibana, Y.; Yukita, W.; Koizumi, M.; Someya, T. Ultraflexible Organic Photonic Skin. *Sci. Adv.* **2016**, *2*, e1501856. [[CrossRef](#)] [[PubMed](#)]
37. Park, S.; Fukuda, K.; Wang, M.; Lee, C.; Yokota, T.; Jin, H.; Jinno, H.; Kimura, H.; Zalar, P.; Matsuhisa, N.; et al. Ultraflexible Near-Infrared Organic Photodetectors for Conformal Photoplethysmogram Sensors. *Adv. Mater.* **2018**, *30*, 1802359. [[CrossRef](#)]
38. Khan, Y.; Han, D.; Pierre, A.; Ting, J.; Wang, X.; Lochner, C.M.; Bovo, G.; Yaacobi-Gross, N.; Newsome, C.; Wilson, R.; et al. A Flexible Organic Reflectance Oximeter Array. *Proc. Natl. Acad. Sci. USA* **2018**, *115*, E11015–E11024. [[CrossRef](#)] [[PubMed](#)]
39. Khan, Y.; Han, D.; Ting, J.; Ahmed, M.; Nagisetty, R.; Arias, A.C. Organic Multi-Channel Optoelectronic Sensors for Wearable Health Monitoring. *IEEE Access* **2019**, *7*, 128114–128124. [[CrossRef](#)]
40. Xu, H.; Liu, J.; Zhang, J.; Zhou, G.; Luo, N.; Zhao, N. Flexible Organic/Inorganic Hybrid Near-Infrared Photoplethysmogram Sensor for Cardiovascular Monitoring. *Adv. Mater.* **2017**, *29*, 1700975. [[CrossRef](#)] [[PubMed](#)]

41. Lee, H.; Kim, E.; Lee, Y.; Kim, H.; Lee, J.; Kim, M.; Yoo, H.-J.; Yoo, S. Toward All-Day Wearable Health Monitoring: An Ultralow-Power, Reflective Organic Pulse Oximetry Sensing Patch. *Sci. Adv.* **2018**, *4*, eaas9530. [[CrossRef](#)]
42. Kim, H.; Kang, T.-H.; Ahn, J.; Han, H.; Park, S.; Kim, S.J.; Park, M.-C.; Paik, S.; Hwang, D.K.; Yi, H.; et al. Spirally Wrapped Carbon Nanotube Microelectrodes for Fiber Optoelectronic Devices beyond Geometrical Limitations toward Smart Wearable E-Textile Applications. *ACS Nano* **2020**, *14*, 17213–17223. [[CrossRef](#)] [[PubMed](#)]
43. Abay, T.Y. Reflectance Photoplethysmography as Noninvasive Monitoring of Tissue Blood Perfusion. *IEEE Trans. Biomed. Eng.* **2015**, *62*, 9. [[CrossRef](#)]
44. Allen, J. Photoplethysmography and Its Application in Clinical Physiological Measurement. *Physiol. Meas.* **2007**, *28*, R1–39. [[CrossRef](#)]
45. Dorlas, J.C.; Mahieu, H.F. Photoelectric Plethysmography—Some Fundamental Aspects of the Reflection and Transmission Method. *Clin. Phys. Physiol. Meas.* **1981**, *2*, 205–215.
46. Ovidia-Blechman, Z.; Gino, O.; Dandeker, L.; Sheffer, N.; Baltaxe, E.; Aharonson, V. The Feasibility of Flat, Portable and Wireless Device for Non-Invasive Peripheral Oxygenation Measurement over the Entire Body. *J. Biomed. Sci. Eng.* **2016**, *9*, 147–159. [[CrossRef](#)]
47. Buchs, A.; Slovik, Y.; Rapoport, M.; Rosenfeld, C.; Khanokh, B.; Nitzan, M. Right-Left Correlation of the Sympathetically Induced Fluctuations of Photoplethysmographic Signal in Diabetic and Non-Diabetic Subjects. *Med. Biol. Eng. Comput.* **2005**, *43*, 252–257. [[CrossRef](#)]
48. Allen, J.; Oates, C.P.; Lees, T.A.; Murray, A. Photoplethysmography Detection of Lower Limb Peripheral Arterial Occlusive Disease: A Comparison of Pulse Timing, Amplitude and Shape Characteristics. *Physiol. Meas.* **2005**, *26*, 811–821. [[CrossRef](#)]
49. Lochner, C.M.; Khan, Y.; Pierre, A.; Arias, A.C. All-Organic Optoelectronic Sensor for Pulse Oximetry. *Nat. Commun.* **2014**, *5*, 5745. [[CrossRef](#)]
50. Zijlstra, W.G.; Buursma, A. Spectrophotometry of Hemoglobin: Absorption Spectra of Bovine Oxyhemoglobin, Deoxyhemoglobin, Carboxyhemoglobin, and Methemoglobin. *Comp. Biochem. Physiol. B Biochem. Mol. Biol.* **1997**, *118*, 743–749. [[CrossRef](#)]
51. Roggan, A.; Friebel, M.; Dörschel, K.; Hahn, A.; Müller, G. Optical Properties of Circulating Human Blood in the Wavelength Range 400–2500 Nm. *J. Biomed. Opt.* **1999**, *4*, 36. [[CrossRef](#)]
52. Gharahbaghian, L.; Massoudian, B.; DiMassa, G. Methemoglobinemia and Sulfhemoglobinemia in Two Pediatric Patients after Ingestion of Hydroxylamine Sulfate. *West. J. Emerg. Med.* **2009**, *10*, 197–201. [[PubMed](#)]
53. Yarynovska, I.H.; Bilyi, A.I. *Absorption Spectra of Sulfhemoglobin Derivates of Human Blood*; Coté, G.L., Priezzhev, A.V., Eds.; SPIE: San Jose, CA, USA, 2006; p. 60940G.
54. Le, Q.-T.; Courter, D. Clinical Biomarkers for Hypoxia Targeting. *Cancer Metastasis Rev.* **2008**, *27*, 351–362. [[CrossRef](#)] [[PubMed](#)]
55. Wright, R.O.; Lewander, W.J.; Woolf, A.D. Methemoglobinemia: Etiology, Pharmacology, and Clinical Management. *Ann. Emerg. Med.* **1999**, *34*, 646–656. [[CrossRef](#)]
56. Scherer, G. Carboxyhemoglobin and Thiocyanate as Biomarkers of Exposure to Carbon Monoxide and Hydrogen Cyanide in Tobacco Smoke. *Exp. Toxicol. Pathol.* **2006**, *58*, 101–124. [[CrossRef](#)] [[PubMed](#)]
57. Faivre, B.; Menu, P.; Labrude, P.; Vigneron, C. Hemoglobin Autooxidation/Oxidation Mechanisms and Methemoglobin Prevention or Reduction Processes in the Bloodstream Literature Review and Outline of Autooxidation Reaction. *Artif. Cells Blood Substit. Biotechnol.* **1998**, *26*, 17–26. [[CrossRef](#)]
58. Anderson, R.R.; Parrish, A. Optical Properties of Human Skin. *J. Biomed. Opt.* **2012**, *17*, 090901.
59. Baranoski, G.V.G.; Chen, T.F.; Kimmel, B.W.; Miranda, E.; Yim, D. On the Noninvasive Optical Monitoring and Differentiation of Methemoglobinemia and Sulfhemoglobinemia. *J. Biomed. Opt.* **2012**, *17*, 15. [[CrossRef](#)]
60. Jo, E.-J.; Mun, H.; Kim, M.-G. Homogeneous Immunosensor Based on Luminescence Resonance Energy Transfer for Glycated Hemoglobin (HbA1c) Detection Using Upconversion Nanoparticles. *Anal. Chem.* **2016**, *88*, 2742–2746. [[CrossRef](#)] [[PubMed](#)]
61. Suner, S.; Partridge, R.; Sucov, A.; Valente, J.; Chee, K.; Hughes, A.; Jay, G. Clinical Laboratory in Emergency Medicine. 10. Non-invasive pulse CO-oximetry screening in the emergency department identifies occult carbon monoxide toxicity. *J. Emerg. Med.* **2008**, *34*, 441–450. [[CrossRef](#)]
62. Chee, K.J.; Nilson, D.; Partridge, R.; Hughes, A.; Suner, S.; Sucov, A.; Jay, G. Finding Needles in a Haystack: A Case Series of Carbon Monoxide Poisoning Detected Using New Technology in the Emergency Department. *Clin. Toxicol.* **2008**, *46*, 461–469. [[CrossRef](#)]
63. Coulange, M.; Barthelemy, A.; Hug, F.; Thierry, A.L.; Haro, L.D. Reliability of New Pulse CO-Oximeter in Victims of Carbon Monoxide Poisoning. *Undersea Hyperb. Med.* **2008**, *35*, 107–111.
64. Mansouri, A.; Lurie, A.A. Methemoglobinemia. *Am. J. Hematol.* **1993**, *42*, 7–12. [[CrossRef](#)] [[PubMed](#)]
65. Aravindhnan, N.; Chisholm, D.G. Sulfhemoglobinemia Presenting as Pulse Oximetry Desaturation. *Anesthesiology* **2000**, *93*, 883–884. [[CrossRef](#)]
66. Malone Rubright, S.L.; Pearce, L.L.; Peterson, J. Environmental Toxicology of Hydrogen Sulfide. *Nitric Oxide* **2017**, *71*, 1–13. [[CrossRef](#)]
67. Docherty, S.; Zmuidinaite, R.; Coulson, J.; Besser, M.; Iles, R. The Diagnosis of Sulfated Hemoglobin (SulfHb) Secondary to Sulfur Dioxide Poisoning Using Matrix-Assisted Laser Desorption Time-of-Flight Mass Spectrometry (MALDI-ToF MS)—A Novel Approach to an Unusual Clinical Problem. *Diagnostics* **2020**, *10*, 94. [[CrossRef](#)]

68. Schiemsy, T.; Penders, J.; Kieffer, D. Failing Blood Gas Measurement Due to Methemoglobin Forming Hemoglobin Variants: A Case Report and Review of the Literature. *Acta Clin. Belg.* **2016**, *71*, 167–170. [[CrossRef](#)] [[PubMed](#)]
69. Camp, N.E. Methemoglobinemia. *J. Emerg. Nurs.* **2007**, *33*, 172–174. [[CrossRef](#)] [[PubMed](#)]
70. Petersson, J.; Åkesson, K.; Sundberg, F.; Särnblad, S. Translating Glycated Hemoglobin A1c into Time Spent in Glucose Target Range: A Multicenter Study. *Pediatr. Diabetes* **2019**, *20*, 339–344. [[CrossRef](#)] [[PubMed](#)]
71. Schnell, O.; Crocker, J.B.; Weng, J. Impact of HbA1c Testing at Point of Care on Diabetes Management. *J. Diabetes Sci. Technol.* **2017**, *11*, 611–617. [[CrossRef](#)]
72. O'Connor, P.J.; Desai, J.R.; Butler, J.C.; Kharbanda, E.O.; Sperl-Hillen, J.M. Current Status and Future Prospects for Electronic Point-of-Care Clinical Decision Support in Diabetes Care. *Curr. Diab. Rep.* **2013**, *13*, 172–176. [[CrossRef](#)]
73. John, A.S.; Davis, T.M.E.; Goodall, I.; Townsend, M.A.; Price, C.P. Nurse-Based Evaluation of Point-of-Care Assays for Glycated Haemoglobin. *Clin. Chim. Acta* **2006**, *365*, 257–263. [[CrossRef](#)]
74. Knaebel, J.; Irvin, B.R.; Xie, C.Z. Accuracy and Clinical Utility of a Point-of-Care HbA1c Testing Device. *Postgrad. Med.* **2013**, *125*, 8. [[CrossRef](#)]
75. Ma, X.-L.; Chen, Z.; Zhu, J.-J.; Shen, X.-X.; Wu, M.-Y.; Shi, L.-P.; Du, L.-Z.; Fu, J.-F.; Shu, Q. Management Strategies of Neonatal Jaundice during the Coronavirus Disease 2019 Outbreak. *World J. Pediatr.* **2020**, *16*, 247–250. [[CrossRef](#)] [[PubMed](#)]
76. Shapiro, S.M.; Riordan, S.M. Review of Bilirubin Neurotoxicity II: Preventing and Treating Acute Bilirubin Encephalopathy and Kernicterus Spectrum Disorders. *Pediatr. Res.* **2020**, *87*, 332–337. [[CrossRef](#)]
77. Bent, B. Investigating Sources of Inaccuracy in Wearable Optical Heart Rate Sensors. *NPJ Digit. Med.* **2020**, *3*, 18. [[CrossRef](#)]
78. Wei, P.; Yang, X.; Cao, Z.; Guo, X.-L.; Jiang, H.; Chen, Y.; Morikado, M.; Qiu, X.; Yu, D. Flexible and Stretchable Electronic Skin with High Durability and Shock Resistance via Embedded 3D Printing Technology for Human Activity Monitoring and Personal Healthcare. *Adv. Mater. Technol.* **2019**, *4*, 1900315. [[CrossRef](#)]
79. Blakers, A.; Zin, N.; McIntosh, K.R.; Fong, K. High Efficiency Silicon Solar Cells. *Energy Procedia* **2013**, *33*, 1–10. [[CrossRef](#)]
80. Park, J.H.; Koo, H.Y.; Kim, S.B.; Choi, S.J.; Lee, J.C. Study on Laser Pyrolysis to Control Silicon Nanocrystal Formation for Novel Photovoltaic Applications. In Proceedings of the 2011 37th IEEE Photovoltaic Specialists Conference, Seattle, WA, USA, 19–24 June 2011; pp. 003065–003067.
81. Stelzner, T.; Pietsch, M.; Andrä, G.; Falk, F.; Ose, E.; Christiansen, S. Silicon Nanowire-Based Solar Cells. *Nanotechnology* **2008**, *19*, 295203. [[CrossRef](#)] [[PubMed](#)]
82. Becker, L. Influence of IR Sensor Technology on the Military and Civil Defense. In *Proceedings Volume 6127, Quantum Sensing and Nanophotonic Devices III*; Razeghi, M., Brown, G.J., Eds.; SPIE: San Jose, CA, USA, 2006; p. 61270S.
83. Kim, J.; Hwang, J.; Song, K.; Kim, N.; Shin, J.C.; Lee, J. Ultra-Thin Flexible GaAs Photovoltaics in Vertical Forms Printed on Metal Surfaces without Interlayer Adhesives. *Appl. Phys. Lett.* **2016**, *108*, 253101. [[CrossRef](#)]
84. Wagner, A.M.; Knipe, J.M.; Orive, G.; Peppas, N.A. Quantum Dots in Biomedical Applications. *Acta Biomater.* **2019**, *94*, 44–63. [[CrossRef](#)] [[PubMed](#)]
85. Lee, G.-H.; Moon, H.; Kim, H.; Lee, G.H.; Kwon, W.; Yoo, S.; Myung, D.; Yun, S.H.; Bao, Z.; Hahn, S.K. Multifunctional Materials for Implantable and Wearable Photonic Healthcare Devices. *Nat. Rev. Mater.* **2020**, *5*, 149–165. [[CrossRef](#)] [[PubMed](#)]
86. Gan, X.; Shiue, R.-J.; Gao, Y.; Meric, I.; Heinz, T.F.; Shepard, K.; Hone, J.; Assefa, S.; Englund, D. Chip-Integrated Ultrafast Graphene Photodetector with High Responsivity. *Nat. Photonics* **2013**, *7*, 883–887. [[CrossRef](#)]